Modulation of the primary auditory thalamus when recognising speech with background noise

Abbreviated Title: vMGB modulation for speech in noise recognition

Paul Glad Mihai[1,2], Nadja Tschentscher[3], Katharina von Kriegstein[1]

[1]Chair of Cognitive and Clinical Neuroscience, Faculty of Psychology, Technische Universität Dresden, 01187 Dresden, Germany

[2]Max Planck Institute for Cognitive and Brain Sciences, 4103 Leipzig, Germany

[3]Research Unit Biological Psychology, Department of Psychology, Ludwig-Maximilians-University Munich, 80802 Munich, Germany

Corresponding author: Katharina von Kriegstein, katharina.von_kriegstein @ tu-dresden.. de

Number of pages: 49

Number of figures: 6

Number of tables: 1

Number of words Abstract: 247

Number of words Introduction: 649

Number of words Discussion: 1475

Conflict of Interest Statement: The authors declare no competing financial interests.

Acknowledgements: The study was funded by the European Research Council ERC Consolidator Grant SENSOCOM (647051) and the Max Planck Society.

Abstract

Recognising speech in background noise is a strenuous daily activity, yet most humans can master it. An explanation of how the human brain deals with such sensory uncertainty during speech recognition is to-date missing. Previous work has shown that recognition of speech without background noise involves modulation of the auditory thalamus (medial geniculate body, MGB): There are higher responses in left MGB for speech recognition tasks that require tracking of fast-varying stimulus properties in contrast to relatively constant stimulus properties (e.g., speaker identity tasks) despite the same stimulus input. Here we tested the hypotheses that (i) this task-dependent modulation for speech recognition increases in parallel with the sensory uncertainty in the speech signal, i.e., the amount of background noise and that (ii) this increase is present in the ventral MGB, which corresponds to the primary sensory part of the auditory thalamus. In accordance with our hypothesis, we show—by using ultra-high-resolution functional magnetic resonance imaging in human participants—that the task-dependent modulation of the left vMGB for speech is particularly strong when recognizing speech in noisy listening conditions in contrast to situations where the speech signal is clear. Exploratory analyses showed that this finding was specific to the left vMGB; it was not present in the right vMGB or the midbrain structure of the auditory pathway (left inferior colliculus, IC). The results imply that speech in noise recognition is supported by modifications at the level of the subcortical sensory pathway providing driving input to the auditory cortex.

Significance Statement

Speech recognition in noisy environments is a challenging everyday task. One reason why humans can master this task is the recruitment of additional cognitive resources as reflected in recruitment of non-language cerebral cortex areas. Here, we show that also modulation in the primary sensory pathway is specifically involved in speech in noise recognition. We found that the left primary sensory thalamus (ventral medial geniculate body, vMGB) is more involved when recognizing speech signals as opposed to a control task (speaker identity recognition) when heard in background noise vs. when the noise was absent. This finding implies that the brain optimises sensory processing in subcortical sensory pathway structures in a task-specific manner to deal with speech recognition in noisy environments.

Author contributions: PGM: collected data, analysed data, interpreted results, wrote the manuscript, edited the manuscript. NT: conceptualised experiment, programmed experiment, edited the manuscript. KvK: conceptualised experiment, interpreted results, wrote the manuscript, edited the manuscript.

1. Introduction

Roaring engines, the hammering from a construction site, the chit-chat of many children in a classroom are just some examples of background noises which continuously accompany us. Nevertheless, humans have a remarkable ability to hear and understand the conversation partner, even under these severe listening conditions (Cherry, 1953) .

Understanding speech in noise is a complex task that involves both sensory and cognitive

processes (Moore et al., 1985; Bregman, 1994; Best et al., 2007; Sayles and Winter, 2008; Shinn-Cunningham and Best, 2008; Song et al., 2010; Adank, 2012; Bronkhorst, 2015; Peelle, 2018; Alavash et al., 2019). However, a more mechanistic explanation of why the human brain masters speech recognition in noise relatively well is missing. Such explanation could advance the understanding of difficulties with speech-in-noise perception in several clinical populations such as age-related hearing impairment (Schoof and Rosen, 2016), autism spectrum disorder (Alcántara et al., 2004), auditory processing disorder (Iliadou et al., 2017), or developmental dyslexia (Chandrasekaran et al., 2009; Ziegler et al., 2009). Furthermore, a more mechanistic understanding of speech-in-noise recognition might also trigger new insight on why artificial speech recognition systems still have difficulties with noisy situations (Scharenborg, 2007; Gupta et al., 2016).

One mechanistic account of brain function that attempts to explain how the human brain deals with uncertainty in the stimulus input is the Bayesian brain hypothesis. It assumes that the brain represents information probabilistically and uses an internal generative model and predictive coding for the most effective processing of sensory input (Knill and Pouget, 2004; Friston, 2005; Kiebel et al., 2008; Friston and Kiebel, 2009). Such type of processing has the potential to explain why the human brain is robust to sensory uncertainty, e.g., when recognising speech despite noise in the speech signal (Srinivasan et al., 1982; Knill and Pouget, 2004). Although predictive coding is often discussed in the context of cerebral cortex organization (Hesselmann et al., 2010; Shipp et al., 2013), it may also be a governing principle of the interactions between cerebral cortex and subcortical sensory pathway structures

84 (Mumford, 1992; von Kriegstein et al., 2008; Huang and Rao, 2011; Bastos et al., 2012; Adams
85 et al., 2013; Seth and Friston, 2016).

86 In humans, responses in the auditory sensory thalamus (medial geniculate body, MGB) are
87 higher for speech tasks (that emphasise recognition of fast-varying speech properties) in
88 contrast to control tasks (that require recognition of relatively constant properties of the
89 speech signal, such as the speaker identity or the sound intensity level). This response
90 difference holds even if the stimulus input is the same (von Kriegstein et al., 2008; Díaz et al.,
91 2012), indicating that the effect is dependent on the specific tasks. We will therefore call it
92 task-dependent modulation in the following. The task-dependent modulation seems to be
93 behaviourally relevant for speech recognition: performance level in auditory speech
94 recognition positively correlates with the amount of task-dependent modulation in the MGB
95 of the left hemisphere (von Kriegstein et al., 2008; Mihai et al., 2019). This behaviourally
96 relevant task-dependent modulation was located in the ventral part of the MGB (vMGB),
97 which is the primary subsection of the MGB (Mihai et al., 2019). These findings have been
98 interpreted by extending the Bayesian brain hypothesis to cortico-subcortical interactions:
99 cerebral cortex areas provide dynamic predictions about the incoming sensory input to the
100 sensory thalamus to optimally encode the trajectory of the fast-varying and predictable
101 speech input (von Kriegstein et al., 2008; Díaz et al., 2012). If this is the case, then the task-
102 dependent modulation of the vMGB should be especially strong when the fast dynamics of
103 speech have to be recognised in conditions with high sensory uncertainty (Yu and Dayan,
104 2005; Feldman and Friston, 2010; Díaz et al., 2012; Van de Cruys et al., 2014), for example
105 when the incoming signal is disturbed (Yu and Dayan, 2005; Friston and Kiebel, 2009;

106 Feldman and Friston, 2010; Gordon et al., 2017). In the present study we tested this
107 hypothesis.

108 2. Materials and Methods

109 2.1 Study overview

110 Presentation of speech in background noise is an ecologically valid way to increase
111 uncertainty about the speech input (Chandrasekaran and Kraus, 2010a). We, therefore,
112 tested, whether the task-dependent modulation of the left vMGB for speech is higher when
113 the speech stimuli are embedded in a noisy as opposed to a clear background. We used ultra-
114 high field functional magnetic resonance imaging (fMRI) at 7 T and a design that has been
115 shown to elicit task-dependent modulation of the MGB in previous studies (von Kriegstein et
116 al., 2008; Díaz et al., 2012). We complemented the design by a noise factor: the speech stimuli
117 (i.e., vowel-consonant-vowel syllables) were presented with and without background noise
118 (Figure 1). The experiment was a 2 × 2 factorial design with the factors task (speech task,
119 speaker task) and noise (noise, clear). To test our hypothesis, we performed a task × noise
120 interaction analysis with the prediction that the task-dependent modulation of the left vMGB
121 increases with decreasing signal-to-noise ratios (i.e., increasing uncertainty about the speech
122 sounds). We focused on the left vMGB for two reasons. First, its response showed behavioural
123 relevance for speech recognition in previous studies (von Kriegstein et al., 2008; Mihai et al.,
124 2019). Second, developmental dyslexia – a condition that is often associated with speech-in-
125 noise recognition difficulties (Chandrasekaran et al., 2009; Ziegler et al., 2009) – has been
126 associated with reduced task-dependent modulation of the left MGB in comparison to

127 controls (Díaz et al., 2012) as well as decreased connections between left MGB and left
128 auditory association cortex (Tschentscher et al., 2019).

129 In addition to testing our main hypothesis, the design also allowed the exploration of the role
130 of the inferior colliculus (IC) – the midbrain station of the auditory sensory pathway – in
131 speech-in-noise recognition.

132 2.2 Participants

133 The Ethics committee of the Medical Faculty, University of Leipzig, Germany, approved the
134 study. We recruited 17 participants (mean age 27.7, SD 2.5 years, 10 female; 15 of these
135 participated in a previous study: Mihai et al., 2019) from the database of the Max Planck
136 Institute for Human Cognitive and Brain Sciences (MPI-CBS), Leipzig, Germany. The sample
137 size was based on the amount of data acquisition time allocated by the MPI-CBS directorial
138 board to the study. The participants were right-handed (as assessed by the Edinburgh
139 Handedness Inventory (Oldfield 1971)), and native German speakers. Participants provided
140 written informed consent. None of the participants reported a history of psychiatric or
141 neurological disorders, hearing difficulties, or current use of psychoactive medications.
142 Normal hearing abilities were confirmed with pure tone audiometry (250 Hz to 8000 Hz;
143 Madsen Micromate 304, GN Otometrics, Denmark) with a threshold equal to and below 25
144 dB). To exclude possible undiagnosed developmental dyslexics, we tested the participant's
145 reading speed and reading comprehension using the German LGVT: 6-12 test (Schneider et
146 al., 2007). The cut-off for both reading scores was set to those levels mentioned in the test
147 instructions as the "lower average and above" performance range (i.e., 26% - 100% of the
148 calculated population distribution). None of the participants performed below the cut off

performance (mean 68.7%, SD 20.6%, lowest mean score: 36%). In addition, participants were tested on rapid automatized naming (RAN) of letters, numbers, and objects (Denckla and Rudel, 1976). The time required to name letters and numbers predicts reading ability and is longer in developmental dyslexics compared with typical readers, whereas the time to name objects is not a reliable predictor of reading ability in adults (Semrud-Clikeman et al., 2000). Participants scored well within the range of control participants for letters (mean 17.25, SD 2.52 s), numbers (mean 16.79, SD 2.63 s), and objects (mean 29.65, SD 4.47 s), based on results from a previous study (Díaz et al., 2012, letters: 16.09, SD 2.60; numbers: 16.49, SD 2.35; objects: 30.84, SD 5.85; age of participants was also comparable 23.5, SD 2.8 years). Furthermore, none of the participants exhibited a clinically relevant number of traits associated with autism spectrum disorder as assessed by the Autism Spectrum Quotient [AQ; mean: 15.9, SD 4.1; cut-off: 32-50; (Baron-Cohen et al., 2001)]. We tested AQ as autism can be associated with difficulties in speech-in-noise perception (Alcántara et al., 2004; Groen et al., 2009). Participants received monetary compensation for participating in the study.

2.2 Stimuli

We recorded 79 different vowel-consonant-vowel (VCV) syllables with an average duration of 784 ms, SD 67 ms. These recordings constitute a subsample from those used in (Mihai et al., 2019). These were spoken by one male voice (age 29 years), recorded with a video camera (Canon Legria HFS10, Canon, Japan) and a Røde NTG-1 microphone (Røde Microphones, Silverwater, NSW, Australia) connected to a pre-amplifier (TubeMP Project Series, Applied Research and Technology, Rochester, NY, USA) in a sound-attenuated room. The sampling rate was 48 kHz at 16 bit. Auditory stimuli were cut and flanked by Hamming windows of 15

171 ms at the beginning and end, converted to mono, and root-mean-square equalised using
172 Python 3.6 (Python Software Foundation, www.python.org). The 79 auditory files were
173 resynthesized with TANDEM-STRAIGHT (Banno et al., 2007) to create three different
174 speakers: 79 auditory files with a vocal tract length (VTL) of 17 cm and glottal pulse rate
175 (GPR) of 100 Hz, 79 with VTL of 16 cm and GPR of 150 Hz, and 79 with VTL of 14 cm and GPR
176 of 300 Hz. This procedure resulted in 237 different auditory stimuli. The parameter choice
177 (VTL and GPR) was motivated by the fact that a VTL difference of 25% and a GPR difference
178 of 45% suffices for listeners to hear different speaker identities (Gaudrain et al., 2009a;
179 Kreitewolf et al., 2014). Additionally, we conducted pilot experiments (12 pilot participants
180 which did not participate in the main experiment) in order to fine-tune the combination of
181 VTL and GPR that resulted in a balanced behavioural accuracy score between the speech and
182 speaker tasks. The pilot experiments were conducted outside the MRI-machine, but included
183 continuous recordings of MRI-gradient noise to simulate a real MRI-environment.

184 We embedded the 237 stimuli in background noise to create the stimuli for the condition
185 with background noise. The background noise consisted of normally distributed random
186 (white) noise filtered with a speech-shaped envelope. We calculated the envelope from the
187 sum of all VCV stimuli presented in the experiment. We used speech-shaped noise as it has a
188 stronger masking effect than stationary random non-speech noise (Carhart et al., 1975).
189 Before each experimental run, the noise was computed and added to the stimuli included in
190 the run with a signal-to-noise ratio (SNR) of 2 dB. The SNR choice was based on a pilot study
191 that showed a performance decrease of at least 5% but no greater than 15% between the
192 clear and noise condition. In the pilot study, we started at an SNR of -10 dB and increased this

value until we converged on an SNR of 2 dB. Calculations were performed in Matlab 8.6 (The Mathworks Inc., Natick, MA, USA) on Ubuntu Linux 16.04 (Canonical Ltd., London, UK).

2.3 Procedure

We conceived the experiment as a 2 × 2 factorial design. The first factor was task (speech, speaker) similar to previous experiments that reported task-dependent modulation of the MGB (von Kriegstein et al., 2008; Díaz et al., 2012; Mihai et al., 2019). The second factor was background noise (clear, noise, Figure 1). Participants listened to blocks of auditory VCV syllables and were asked to perform the two types of tasks: the speech task and the speaker task. In the speech task, participants reported via button press whether the current syllable was different from the previous one (1-back task). In the speaker task, participants reported via button press whether the current speaker was different from the previous one. The blocks had either syllables with background noise (noise condition) or without background noise (clear condition).

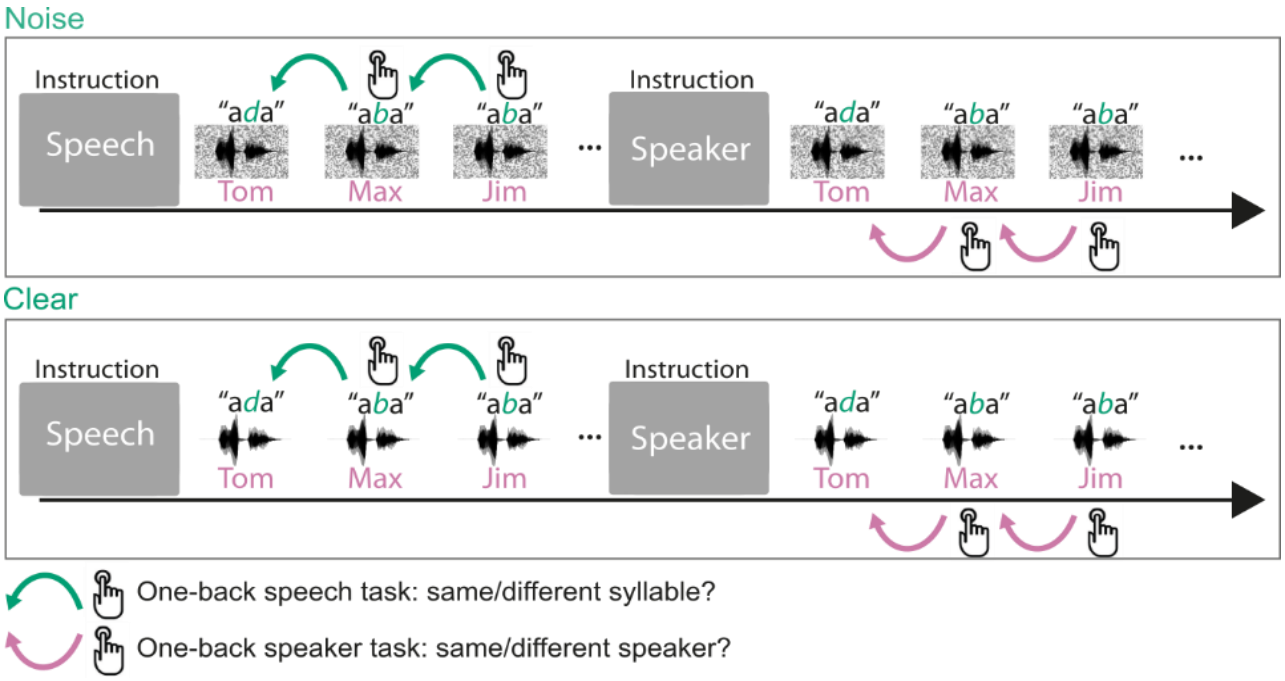

Figure 1. Design and trial structure of the experiment. In the speech task, listeners performed a one-back syllable task. They pressed a button whenever there was a change in syllable in contrast to the immediately preceding one, independent of speaker change. The speaker task used precisely the same stimulus material and trial structure. The task was to press a button when there was a change in speaker identity in contrast to the immediately preceding one, independent of syllable change. The speakers' voices were resynthesized from the recordings of one speaker's voice to only differ in constant speaker individuating features (i.e., the vocal tract length and the fundamental frequency of the voice). This ensured that the speaker task could not be done on dynamic speaker individuating features (e.g., idiosyncrasies in pronunciations of phonemes). An initial task instruction screen informed participants about which task to perform. Participants heard stimuli either with concomitant speech-shaped noise (noise condition) or without background noise (clear condition). Thus the experiment had four conditions: speech task/noise, speaker task/noise, speech task/clear, speaker task/clear. Stimuli in the speech and speaker tasks were precisely identical.

Task instructions were presented for two seconds before each block and consisted of white written words on a black background (German words "Silbe" for syllable indicating the speech task, and "Person" for person indicating the speaker task). After the instruction, the block of syllables started (Figure 1). Each block contained twelve stimuli. Each stimulus had a duration of approximately 784 ms, and the stimulus presentation was followed by 400 ms

of silence. Within one block both syllables and speakers changed at least twice, with a theoretical maximum of nine changes. The theoretical maximum was derived from random sampling of seven instances from three possible change types: no change, speech change, speaker change, and change of speech and speaker. The average length of a block was 15.80 seconds, SD 0.52 seconds. The presentation of the stimuli was randomized and balanced with regard to the amount of speaker identity and syllable changes within a block. The same block containing speaker identity changes also contained syllable changes. These blocks were repeated, once with the instruction to perform the speaker identity task and the other time to perform the speech task. This procedure ensured that subjects heard exactly the same stimuli while performing the two different tasks.

The experiment was divided into four runs. The first three runs had a duration of 12:56 min and included 40 blocks: 10 for each of the four conditions (speech task/noise, speaker task/noise, speech task/clear, speaker task/clear). A fourth run had a duration of 6:32 min and included 20 blocks (5 for each of the four conditions). For two participants, only the first three runs were recorded due to time constraints. Participants could rest for one minute between runs.

Participants were familiarised with the three speakers' voices to ensure that they could perform the speaker-identity task of the main experiment. The speaker familiarisation took place 30 minutes before the fMRI experiment. It consisted of a presentation of the speakers and a test phase. In the presentation phase, the speakers were presented in six blocks, each containing nine pseudo-randomly chosen VCV stimuli from the 237 total. Each block

contained one speaker-identity only. Participants were alerted to the onset of a new speaker identity block by the presentation of white words on a black screen indicating speaker 1, speaker 2, or speaker 3. Participants listened to the voices with the instruction to memorise the speaker's voice. In the following test phase participants were presented with four blocks of nine trials that each contained randomly chosen syllable pairs spoken by the three speakers. The syllable pairs could be from the same or a different speaker. We asked participants to indicate whether the speakers of the two syllables were the same by pressing keypad buttons "1" for yes and "2" for no. Participants received visual feedback for correct (the green flashing German word for correct: "Richtig") and incorrect (the red flashing German word for incorrect: "Falsch") answers. The speaker familiarisation consisted of three 2:50 min runs (each run contained one presentation and one test phase). If participants scored below 80% on the last run, they performed an additional run until they scored above 80%. All participants exceeded the 80% cut-off value.

The experiments were programmed in the Matlab Psychophysics Toolbox [Psychtoolbox-3, www.psychtoolbox.com (Brainard, 1997)] running on Matlab 8.6 (The Mathworks Inc., Natick, MA, USA) on Ubuntu Linux 16.04 (Canonical Ltd., London, UK). The sound was delivered through a MrConfon amplifier and headphones (manufactured 2008; MrConfon GmbH, Magdeburg, Germany).

2.4 Data Acquisition and Processing

MRI data were acquired using a Siemens Magnetom 7 T scanner (Siemens AG, Erlangen, Germany) with an 8-channel head coil. We convened on the 8-channel coil, due to its spaciousness which allowed the use of higher quality headphones (manufactured 2008;

271 MrConfon GmbH, Magdeburg, Germany). Functional MRI data were acquired using echo-
272 planar imaging (EPI) sequences. We used partial brain coverage with 30 slices. The volume
273 was oriented in parallel to the superior temporal gyrus such that the slices encompassed the
274 MGB, the inferior colliculi (IC), and the Heschl's gyrus.

275 The EPI sequences had the following acquisition parameters: TR = 1600 ms, TE = 19 ms, flip
276 angle 65°, GRAPPA (Griswold et al., 2002) with acceleration factor 2, 33% phase
277 oversampling, matrix size 88, field of view (FoV) of 132 mm x 132 mm, phase partial Fourier
278 6/8, voxel size 1.5 mm isotropic resolution, interleaved acquisition, anterior to posterior
279 phase-encode direction. The first three runs consisted of 485 volumes (12:56 min), and the
280 fourth run consisted of 245 volumes (6:32 min). During functional MRI data acquisition, we
281 also acquired physiological values (heart rate, and respiration rate) using a BIOPAC MP150
282 system (BIOPAC Systems Inc., Goleta, CA, USA).

283 To address geometric distortions in EPI images we recorded gradient echo based field maps
284 which had the following acquisition parameters: TR = 1500 ms, TE1 = 6.00 ms, TE2 = 7.02
285 ms, flip angle 60°, 0% phase oversampling, matrix size 100, FoV 220 mm x 220 mm, phase
286 partial Fourier off, voxel size 2.2 mm isotropic resolution, interleaved acquisition, anterior to
287 posterior phase-encode direction. Resulting images from field map recordings were two
288 magnitude images and one phase difference image.

289 Structural images were recorded using an MP2RAGE (Marques et al., 2010) T1 protocol: 700
290 µm isotropic resolution, TE = 2.45ms, TR = 5000 ms, TI1 = 900 ms, TI2 = 2750 ms, flip angle
291 1 = 5°, flip angle 2 = 3°, FoV 224 mm × 224 mm, GRAPPA acceleration factor 2, duration 10:57
292 min.

2.5 Behavioural Data Analysis

Button presses (hits, misses) were binomially distributed, and were thus modeled using a binomial logistic regression which predicts the probability of correct button presses based on four independent variables (speech task/noise, speaker task/noise, speech task/clear, speaker task/clear) in a Bayesian framework (McElreath, 2018).

To pool over participants and runs we modelled the correlation between intercepts and slopes. For the model implementation and data analysis, we used PyMC3 3.5 (Salvatier et al., 2016), a probabilistic programming package for Python 3.6. We sampled with a No-U-Turn Sampler (Hoffman and Gelman, 2014) with four parallel chains. Per chain, we had 5,000 samples with 5,000 as warm-up. The data entering the model was mean centered by subtracting the mean and dividing by two standard deviations (Gelman and Hill, 2006). This transformation does not change the fit of the linear model and the coefficients are interpretable in comparison to the mean of the data. The reason behind this transformation is the faster and more accurate convergence of the Markov Chain sampling (McElreath, 2018).

There were the following effects of interest: main effects (clear - noise, speech task - speaker task), the interaction (speech task/ noise - speaker task/ noise) - (speech task/ clear - speaker task/ clear), simple main effects (speech task/ noise - speaker task/ noise, speech task/ clear - speaker task/ clear). For the effects of interest, we calculated means from the posterior distributions and 95% highest posterior density intervals (HDP). The HPD is the probability that the mean lies within the interval (Gelman et al., 2013; McElreath, 2018), this means that we are 95% sure the mean lies within the specified interval bounds. If the

posterior probability distribution of odds ratios does not strongly overlap one (i.e., the HPD excludes one), then it is assumed that there is a detectable difference between conditions (Bunce and McElreath, 2017; McElreath, 2018).

The predictors included in the behavioural data model were: task (x_S:1 = speech task, 0 = speaker task), and background noise (x_N: 1 = noise, 0 = clear). We also included the two-way interaction of task and noise condition. Because data were collected across participants and runs, we included random effects for both of these in the logistic model. Furthermore, since ~11% of the data exhibited ceiling effects (i.e., some participants scored at the highest possible level) which would result in underestimated means and standard deviations (Uttl, 2005), we treated these data as right-censored and modeled them using a Potential class (Lauritzen et al., 1990; Jordan, 1998) as implemented in PyMC3. This method integrates the censored values using the log of the complementary normal cumulative distribution function (Gelman et al., 2013; McElreath, 2018). In essence, we sampled twice, once for the observed values without the censored data points, and once for the censored values only. The model is described below.

$$L_{i,j} \sim Binomial(1, p_{i,j})$$

$$p_{i,j} = \begin{cases} p^*_{i,j}, & \text{for } p^*_{i,j} < c \\ c, & \text{for } p^*_{i,j} \geq c \end{cases}$$

$$logit(p^*_{i,j}) = A_{i,j} + B_{S,i,j}x_S + B_{N,i,j}x_N + B_{SN,i,j}x_S x_N, \text{for } i = 1, \ldots, I; j = 1, \ldots, J$$

$$A_{i,j} = \alpha + \alpha_{participant[i]} + \alpha_{run[j]}$$

$$B_{S,i,j} = \beta_S + \beta_{S,participant[i]} + \beta_{S,run[j]}$$

$$B_{N,i,j} = \beta_N + \beta_{N,participant[i]} + \beta_{N,run[j]}$$

$$B_{SN,i,j} = \beta_{SN} + \beta_{SN,participant[i]} + \beta_{SN,run[j]}$$

$$\begin{bmatrix} \alpha_{participant} \\ \beta_{S,participant} \\ \beta_{N,participant} \\ \beta_{SN,participant} \end{bmatrix} \sim MVNormal\left(\begin{bmatrix} \alpha \\ \beta_S \\ \beta_N \\ \beta_{SN} \end{bmatrix}, S_{participant}\right)$$

$$\begin{bmatrix} \alpha_{run} \\ \beta_{S,run} \\ \beta_{N,run} \\ \beta_{SN,run} \end{bmatrix} \sim MVNormal\left(\begin{bmatrix} \alpha \\ \beta_S \\ \beta_N \\ \beta_{SN} \end{bmatrix}, S_{run}\right)$$

$$S_{subject} = \begin{bmatrix} \sigma_\alpha & 0 & 0 & 0 \\ 0 & \sigma_{\beta_S} & 0 & 0 \\ 0 & 0 & \sigma_{\beta_N} & 0 \\ 0 & 0 & 0 & \sigma_{\beta_{SN}} \end{bmatrix} R_{subject} \begin{bmatrix} \sigma_\alpha & 0 & 0 & 0 \\ 0 & \sigma_{\beta_S} & 0 & 0 \\ 0 & 0 & \sigma_{\beta_N} & 0 \\ 0 & 0 & 0 & \sigma_{\beta_{SN}} \end{bmatrix}$$

$$S_{run} = \begin{bmatrix} \sigma_\alpha & 0 & 0 & 0 \\ 0 & \sigma_{\beta_S} & 0 & 0 \\ 0 & 0 & \sigma_{\beta_N} & 0 \\ 0 & 0 & 0 & \sigma_{\beta_{SN}} \end{bmatrix} R_{run} \begin{bmatrix} \sigma_\alpha & 0 & 0 & 0 \\ 0 & \sigma_{\beta_S} & 0 & 0 \\ 0 & 0 & \sigma_{\beta_N} & 0 \\ 0 & 0 & 0 & \sigma_{\beta_{SN}} \end{bmatrix}$$

$$\alpha \sim Normal(0,5)$$

$$\beta_S \sim Normal(0,5)$$

$$\beta_N \sim Normal(0,5)$$

$$\beta_{SN} \sim Normal(0,5)$$

$$(\sigma_{participant}, \sigma_{run}) \sim HalfCauchy(1)$$

$$\sigma_{corr,participant} \sim HalfCauchy(1)$$

$$\sigma_{corr,run} \sim HalfCauchy(1)$$

$$R_{participant} \sim LKJcorr(4, \sigma_{corr,participant})$$

$$R_{run} \sim LKJcorr(4, \sigma_{corr,run})$$

I represents the participants and *J* the runs. The model is compartmentalized into sub-models for the intercepts and slopes. $A_{i,j}$ is the sub-model for the intercept for observations i, j. Similarly, $B_{S,i,j}$, $B_{N,i,j}$, and $B_{SN,i,j}$ are the sub-models for the speech task – speaker task slope, clear-noise slope and the interaction slope, respectively; $S_{subject}/S_{run}$ are the covariance matrices for participant/run. $R_{subject}/R_{run}$ are the priors for the correlation matrices modelled as LKJ probability densities (Lewandowski et al., 2009). Weakly informative priors for the intercept (α) and additional coefficients (e.g., β_S), random effects for participant and run ($\beta_{S,subject}$, $\beta_{S,run}$), and multivariate priors for participants and runs identify the model by constraining the position of $p_{i,j}$ to reasonable values. Here we used normal distributions as priors. Furthermore, $p_{i,j}$ is defined as the ramp function equal to the proportion of hits when these are known and below the ceiling (c), and set to the ceiling if they are equal to or greater than the ceiling *c.*

We additionally analyzed the reaction times, similarly to the model described above but without consideration of ceiling effects as they are non-existent. Posterior distributions were computed for each condition, and we computed main effects and the interaction between task and noise. If the posterior probability distribution of the difference scores and the

369 interaction does not strongly overlap zero (i.e., the HPD excludes zero), then it is assumed
370 that there is a detectable difference (Bunce and McElreath, 2017; McElreath, 2018).

371

372 2.6 Functional MRI Data Analysis

373 2.6.1 Preprocessing of fMRI data

374 The MP2RAGE images were first segmented using SPM's segment function (SPM 12, version
375 12.6906, Wellcome Trust Centre for Human Neuroimaging, UCL, UK,
376 http://www.fil.ion.ucl.ac.uk/spm) running on Matlab 8.6 (The Mathworks Inc., Natick, MA,
377 USA) in Ubuntu Linux 16.04 (Canonical Ltd., London, UK). The resulting grey and white
378 matter segmentations were summed and binarised to remove voxels that contain air, scalp,
379 skull and cerebrospinal fluid from structural images using the ImCalc function of SPM.

380 We used the template image created for a previous study (Mihai et al., 2019) using structural
381 MP2RAGE images from the 28 participants of that study. We chose this template since 15
382 participants in the current study are included in this image, and the vMGB mask (described
383 below) is in the same space as the template image. The choice of this common template
384 reduces warping artefacts, which would be introduced with a different template, as both the
385 vMGB mask and the functional data of the present study would need to be warped to a
386 common space. The template was created and registered to MNI space with ANTs (Avants et
387 al., 2008) and the MNI152 template provided by FSL 5.0.8 (Smith et al., 2004). All MP2RAGE
388 images were preprocessed with Freesurfer (Fischl et al., 2004; Han and Fischl, 2007) using

389 the recon-all command to obtain boundaries between grey and white matter, which were
390 later used in the functional to structural registration step.

391 Preprocessing and statistical analyses pipelines were coded in nipype 1.1.2 (Gorgolewski et
392 al., 2011). Head motion and susceptibility distortion by movement interaction of functional
393 runs were corrected using the Realign and Unwarp method (Andersson et al., 2001) in SPM
394 12. This step also makes use of a voxel displacement map (VDM), which addresses the
395 problem of geometric distortions in EPI caused by magnetic field inhomogeneity. The VDM
396 was calculated using field map recordings, which provided the absolute value and the phase
397 difference image files, using the FieldMap Toolbox (Jezzard and Balaban, 1995) of SPM 12.
398 Outlier runs were detected using ArtifactDetect (composite threshold of translation and
399 rotation: 1; intensity Z-threshold: 3; global threshold: 8;
400 https://www.nitrc.org/projects/artifact_detect/). Coregistration matrices for realigned
401 functional runs per participant were computed based on each participant's structural image
402 using Freesurfer's BBregister function (register mean EPI image to T1). We used a whole-
403 brain EPI volume as an intermediate file in the coregistration step to avoid registration
404 problems due to the limited FoV of the functional runs. Warping using coregistration
405 matrices (after conversion to the ITK coordinate system) and resampling to 1 mm isovoxel
406 was performed using ANTs. Before model creation, we smoothed the data in SPM12 using a
407 1 mm kernel at full-width half-maximum.

408 ### 2.6.2 Physiological data

409 Physiological data (heart rate and respiration rate) were processed by the PhysIO Toolbox
410 (Kasper et al., 2017) to obtain Fourier expansions of each, in order to enter these into the

411 design matrix (see section 2.6.3 Testing our hypothesis in the left vMGB). Since heartbeats
412 and respiration result in undesired cortical and subcortical artefacts, regressing these out
413 increases the specificity of fMRI responses to the task of interest (Kasper et al., 2017). These
414 artefacts occur in abundance around the thalamus (Kasper et al., 2017).

415 2.6.3 Testing our hypothesis in the left vMGB

416 Models were set up in SPM 12 using the native space data for each participant. We modelled
417 five conditions of interest: speech task/noise, speaker task/noise, speech task/clear, speaker
418 task/clear, and task instruction. Onset times and durations were used to create boxcar
419 functions, which were convolved with the hemodynamic response function (HRF) provided
420 by SPM 12. The design matrix also included the following nuisance regressors: three cardiac,
421 four respiratory, and a cardiac × respiratory interaction regressor. We additionally entered
422 the outlier regressors from the ArtifactDetect step.

423 Parameter estimates were computed for each condition at the first level using restricted
424 maximum likelihood (REML) as implemented in SPM 12. Parameter estimates for each of the
425 four conditions of interest (speech task/noise, speaker task/noise, speech task/clear,
426 speaker task/clear) were registered to the MNI structural template using a two-step
427 registration in ANTs. First, a quick registration was performed on the whole head using rigid,
428 affine and diffeomorphic transformations (using Symmetric Normalization, SyN), and the
429 mutual information similarity metric. Second, the high-quality registration was confined to

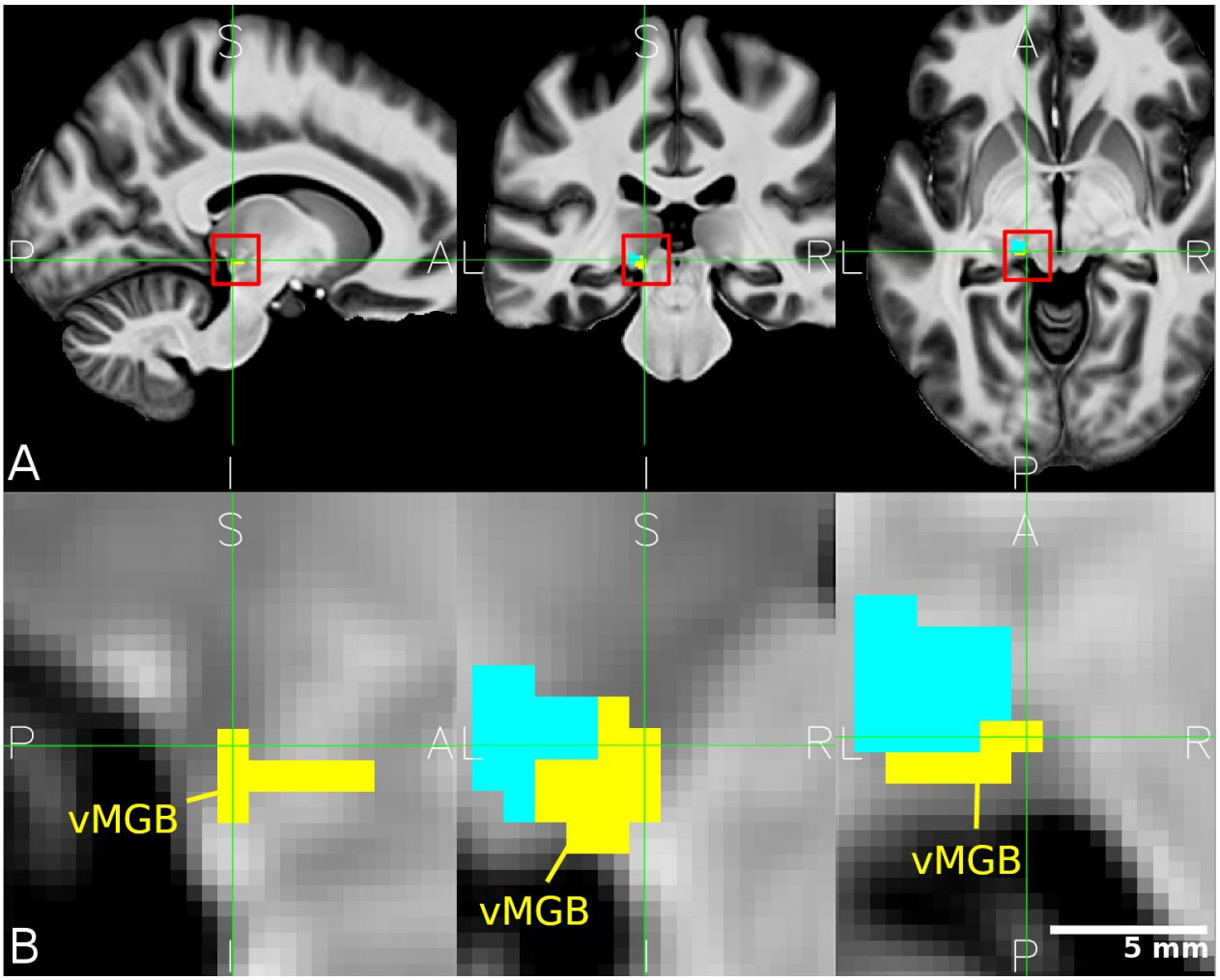

Figure 2. Location of the left MGB masks. (A) The mean structural image across participants (n = 33) in MNI space. The red squares denote the approximate location of the left MGB and encompass the zoomed in view in B. (B) Closeup of the left vMGB (yellow). The tonotopic gradient two is shown in cyan. Panels correspond to sagittal, coronal, and axial slices (P: posterior, A: anterior, S: superior, I: inferior, L: left, R: right).

the volume that was covered by the 30 slices of the EPI images. These volumes include the IC, MGB, and primary and secondary auditory cortices. This step used affine and SyN transformations and mean squares and neighbourhood cross-correlation similarity

measures. We performed the registration to MNI space by linearly interpolating the contrast images using the composite transforms from the high-quality registration.

We extracted parameter estimates for each of the four conditions of interest per participant, averaged over all voxels from the region of interest, i.e., the left vMGB. To locate the left vMGB, we used the mask from (Mihai et al., 2019), which included 15 of the 17 participants of the present study (Figure 2).

We analysed the extracted parameter estimates in a Bayesian framework (McElreath, 2018). The data entering the model was mean centered by subtracting the mean and dividing by two standard deviations (Gelman and Hill, 2006). This transformation does not change the fit of the linear model and the coefficients are interpretable in comparison to the mean of the data. The reason behind this transformation is the faster and more accurate convergence of the Markov Chain sampling (McElreath, 2018). The model was implemented in PyMC3 with a No-U-Turn Sampler with four parallel chains. Per chain, we sampled posterior distributions which had 5000 samples with 5000 as warm-up. The predictors included in the model were: task (x_S: 1 = speech task, 0 = speaker task), and background noise (x_N: 1 = noise, 0 = clear). We also included the two-way interaction of task and noise condition. Because data were collected across participants, it was reasonable to include random effects. To pool over participants, we modelled the correlation between intercepts and slopes over participants. The interaction model is described below.

$$L_i \sim T(\mu_i, \nu, \lambda)$$

$$\mu_i = A_i + B_{S,i}x_S + B_{N,i}x_N + B_{SN,i}x_S x_N, \text{for } i = 1, \ldots, I$$

$$A_i = \alpha + \alpha_{participant[i]}$$

$$B_{S,i} = \beta_S + \beta_{S,participant[i]}$$

$$B_{N,i} = \beta_N + \beta_{N,participant[i]}$$

$$B_{SN,i} = \beta_{SN} + \beta_{SN,participant[i]}$$

$$\begin{bmatrix} \alpha_{participant} \\ \beta_{S,participant} \\ \beta_{N,participant} \\ \beta_{SN,participant} \end{bmatrix} \sim MVNormal\left(\begin{bmatrix} \alpha \\ \beta_S \\ \beta_N \\ \beta_{SN} \end{bmatrix}, S\right)$$

$$S = \begin{bmatrix} \sigma_\alpha & 0 & 0 & 0 \\ 0 & \sigma_{\beta_S} & 0 & 0 \\ 0 & 0 & \sigma_{\beta_N} & 0 \\ 0 & 0 & 0 & \sigma_{\beta_{SN}} \end{bmatrix} R \begin{bmatrix} \sigma_\alpha & 0 & 0 & 0 \\ 0 & \sigma_{\beta_S} & 0 & 0 \\ 0 & 0 & \sigma_{\beta_N} & 0 \\ 0 & 0 & 0 & \sigma_{\beta_{SN}} \end{bmatrix}$$

$$\alpha \sim T(0,1,3)$$

$$\beta_S \sim T(0,1,3)$$

$$\beta_N \sim T(0,1,3)$$

$$\beta_{SN} \sim T(0,1,3)$$

$$(\sigma_{participant}) \sim HalfCauchy(1)$$

$$\sigma_{corr} \sim HalfCauchy(1)$$

$$R \sim LKJcorr(4, \sigma_{corr})$$

$$\nu \sim Exponential(1/29) + 1$$

$$\sigma \sim HalfCauchy(2)$$

$$\lambda = \sigma^{-2}$$

I represents the participants. The model is compartmentalized into sub-models for the intercepts and slopes. A_i is the sub-model for the intercept for observations i. Similarly, $B_{S,i}$, $B_{N,i}$, and $B_{SN,i}$ are the sub-models for the speech task -speaker task slope, clear-noise slope and the interaction slope, respectively; S is the covariance matrix and R is the prior for the correlation matrix modelled as an LKJ probability density (Lewandowski et al., 2009). Weakly informative priors for the intercept (α) and additional coefficients (e.g., β_S), random effects for participant ($\beta_{S,subject}$), and multivariate priors for participants identify the model by constraining the position of μ_i to reasonable values. Here we used Student's-T distributions as priors.

From the model output, we calculated posterior distributions for each condition of interest (speech task/noise, speaker task/ noise, speech task/clear, speaker task/clear). Posterior distributions, in comparison to point estimates, have the advantage of quantifying uncertainty about each parameter. We summarised each posterior distribution using the mean as a point estimate (posterior mean) together with a 95% highest posterior density interval (HPD). The HPD is the probability that the mean lies within the interval (Gelman et al., 2013; McElreath, 2018), e.g., we are 95% sure the mean lies within the specified interval bounds. We computed the following contrasts of interest: interaction (speech task/noise – speaker task/noise) – (speech task/clear – speaker task/clear); simple main effects (speech task/noise – speaker task/noise), (speech task/clear – speaker task/clear); main effect of task (speech task – speaker task). Differences between conditions were converted to effect

498 sizes [Hedges g* (Hedges and Olkin, 1985)]. Hedges g*, like Cohen's d (Cohen, 1988), is a
499 population parameter that computes the difference in means between two variables
500 normalised by the pooled standard deviation with the benefit of correcting for small sample
501 sizes. Based on Cohen (1988), we interpreted effect sizes on a spectrum ranging from small
502 ($g^* \approx 0.2$), to medium ($g^* \approx 0.5$), to large ($g^* \approx 0.8$), and beyond. If the HPD did not overlap
503 zero, we considered this to be a robust effect (Bunce and McElreath, 2017; McElreath, 2018).
504 However, we caution readers that if the HPD includes zero, it does not mean that the effect is
505 missing (Amrhein et al., 2019). Instead, we quantify and interpret the magnitude (by the
506 point estimate) and its uncertainty (by the HPD) provided by the data and our assumptions
507 (Anderson, 2019).

508 ### 2.6.4 Analyses of the left inferior colliculus

509 The study design and acquisition parameters also allowed us to explore the involvement of
510 the IC in speech-in-noise recognition (for a rationale of these exploratory analyses see
511 results, section 3.2.2). To analyse the task × noise interaction and the main effect of task in
512 the bilateral IC we used the same analysis procedures as described for the left vMGB (see
513 section 2.6.3 Testing our hypothesis in the left vMGB). As region of interest, we used the IC
514 masks described in (Mihai et al., 2019) and limited them to the tonotopic parts of the IC, i.e.,
515 the central nucleus (Figure 3), which corresponds to the primary auditory pathway (Davis,
516 2005). We will call it

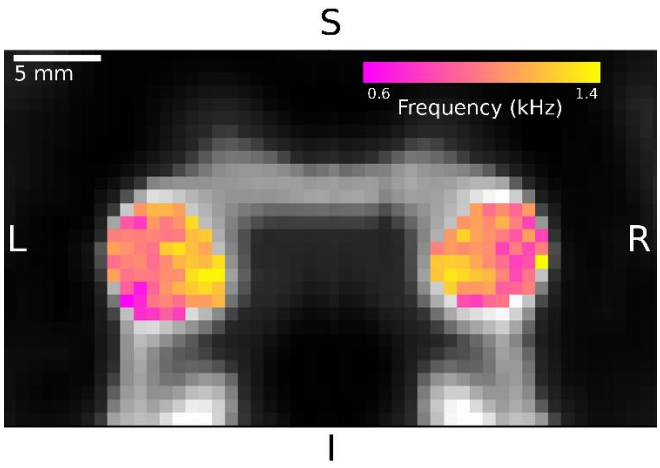

Figure 3. Tonotopy gradients in the inferior colliculi. The colored parts show one slice of the mean tonotopic map across participants in the left and right IC in coronal view (S: superior, I: inferior, L: left, R: right). Individual tonotopies showed high varuability (results not shown). The mean tonotopy revealed a gradient from low frequencies in lateral locations to high frequencies in medial locations (Mihai et al., 2019). The maps were used to construct a region of interest for the central nucleus of the IC (cIC).

cIC in the following. Furthermore, we performed a Pearson's correlation calculation to analyse the correlation (speech - speaker task correlated with speech accuracy score) in the left cIC. The motivation for this test was based on similar correlations (i.e., speech – control task correlated with speech accuracy score) found in two previous experiments in the left cIC (von Kriegstein et al., 2008 experiment 1 and 2) (for further details see results, section 3.2.2).

3. Results

3.1 Behavioural results

3.1.1 Accuracy

Participants performed well above chance level in all four conditions (> 82% correct; Table 1; Figure 4A).

Table 1. The proportion of hits for each of the four conditions in the experiment. HDP: highest posterior density interval.

	Speech task/ Noise	**Speaker task/ Noise**	**Speech task/ Clear**	**Speaker task/ Clear**
Hit rate [95% HPD]	0.82 [0.62, 0.95]	0.87 [0.74, 0.96]	0.92 [0.83, 0.98]	0.90 [0.81, 0.97]

Performing the tasks with background noise was more difficult than the conditions without background noise for both the speech and the speaker task (Figure 4B, for details on statistics, see figure and legend). The rate of hits in the speech task was the same as in the speaker task (Figure 4C). There was a detectable interaction between task and noise (Figure 4D/E), but simple main effects (i.e., speech task/noise - speaker task/noise (Figure 4F) and speech task/clear - speaker task/clear (Figure 4G)) were not present. We also observed ceiling effects in 11% of the cases, which were modeled accordingly (Materials and Methods, section 2.5).

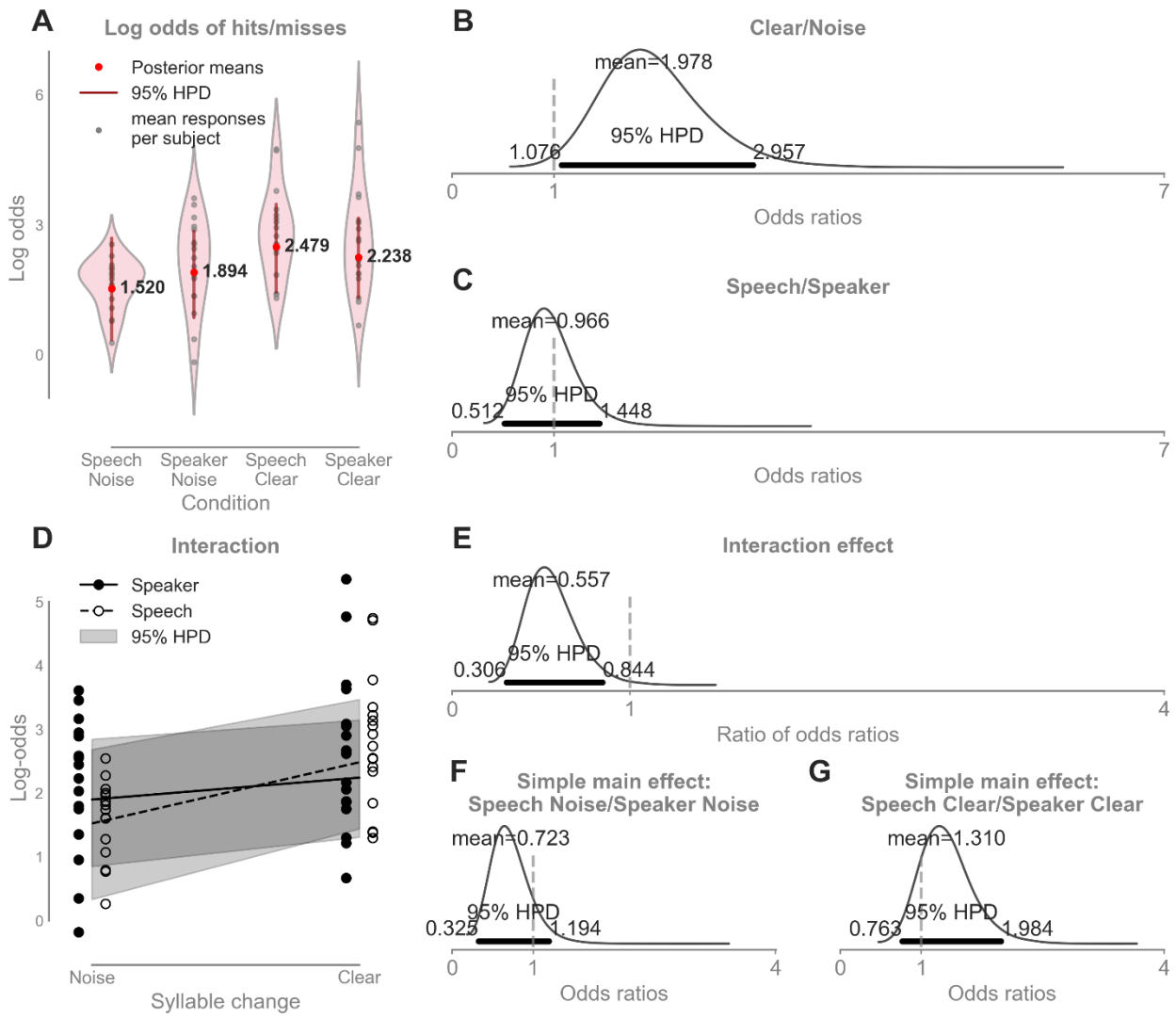

Figure 4. Behavioural results. We performed a binomial logistic regression to compute the rate of hits and misses in each condition because behavioural data were binomially distributed. For this reason, results are reported in log odds and odds ratios. The results showed a detectable main effect of noise and interaction between noise and task. There was no main effect of task,

and no detectable simple main effects (speech task/noise - speaker task/noise; speech task/clear - speaker task/clear). ***A.*** *Log odds of hits and misses for each condition. The grey dots indicate mean responses for individual participants, the red dots and accompanying numbers denote the posterior mean per condition, and the dark red lines demarcate the 95% highest posterior density interval (HPD). The rate of hits compared to misses is plotted on a log scale to allow for a linear representation.* ***B.*** *Mean odds ratio for the clear and noise conditions. The odds of hits in the clear condition were on average twice as high as in the noise condition (the mean odds ratio was 1.978 [1.076, 2.957]). The HPD excluded 1 and indicated a detectable difference between conditions: No difference would be assumed if the odds ratio was 1 (50/50 chance or 1:1 ratio; Chen, 2003).* ***C.*** *Mean odds ratio for the speech task - speaker task conditions. The mean odds ratio was ~1 indicating no difference between the speech and speaker task conditions.* ***D****. Visualization of the interaction (task × noise) as a comparison of slopes with 95% HPD.* ***E****. The ratio of odds ratios of the simple main effects speech task/noise - speaker task/noise and speech task/clear - speaker task/clear. The mean and 95% HPD was 0.557 [0.306, 0.844]. The HPD excluded 1 indicating an interaction effect.* ***F****. Mean odds ratio for the simple main effect speech task/noise - speaker task/noise. The rate of hits in the speech task/noise condition was on average ~1/3 lower than the rate of hits in the speaker task/noise condition; however, the HPD strongly overlapped 1 indicating that there was no difference between conditions.* ***G****. Mean odds ratio for the simple main effect speech task/clear - speaker task/clear. The rate of hits in the speech task/clear condition was on average ~1/3 higher than the rate of hits in the speaker task/clear condition; however, the HPD strongly overlapped 1 indicating that there was no detectable difference between conditions.*

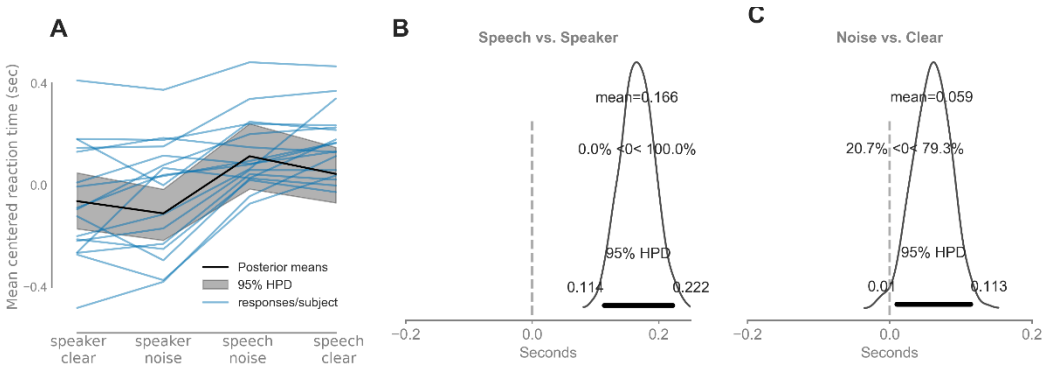

Figure 5. Reaction times results. **A.** Mean centered reaction times for each condition. The blue lines indicate individual average reaction times, the black line denotes the estimated reaction time per condition averaged over participants and runs, the grey shaded area denotes the 95% highest posterior density interval (HPD). **B.** Mean reaction time difference between the Speech and Speaker task. On average, participants took 0.166 [0.114, 0.222] s longer to react in the Speech than to the Speaker task. **C.** Mean reaction time difference between the Noise and the Clear condition. On average, participants took 0.059 [0.010, 0.113] s longer to react during the Noise vs. Clear condition. There was no task x noise interaction.

3.1.2 Reaction times

The reaction times analysis showed that for the speech task participants required on average 0.166 [0.114, 0.222] s longer to react than for the speaker task (Figure 5). This effect is explained by the fact that VCV syllables had constant vowels and only the consonants changed within one block. Therefore, listeners had to wait for the consonant to detect a change. Whereas, for the speaker identitiy task the glottal pulse rate is the strongest cue, and is immediately decoded (Gaudrain et al., 2009b). The difference in reaction times between the noise and clear condition was on average 0.059 [0.010, 0.113] s. This difference showed that the noise condition required a minimal amount of extra processing time, yet this

597 difference was on average very small. Lastly, the task x noise interaction was on average
598 0.022 s with the HPD overlapping zero ([-0.028, 0.076] s), which is not a meaningful effect.

599 3.2 fMRI Results

600 3.2.1 The task-dependent modulation of left vMGB was increased for recognizing
601 speech-in-noise in contrast to the clear speech condition

602 We localised the left vMGB based on an independent functional localizer (Figure 6B).
603 Following our hypothesis, there was increased BOLD response for the task × noise interaction
604 [(speech task/noise - speaker task/noise) - (speech task/clear - speaker task/clear)] in the
605 left vMGB (Figure 6A/B). The interaction effect had a mean large effect size ranging across
606 participants from a small effect to a very large effect (g*=2.549 [0.211, 5.066]; Figure 6C and
607 D). The 95% HPD of the interaction effect excluded 0, indicating that this was a robust effect
608 (Bunce and McElreath, 2017; McElreath, 2018). Simple main effect analyses showed that the
609 direction of the interaction was as expected. The speech task/noise condition yielded higher
610 left vMGB responses in contrast to the speaker task/noise condition, ranging from a medium
611 to a very large effect across participants (g* = 1.104 [0.407, 1.798]; Figure 6E). Conversely,
612 the left vMGB response difference between the speech task and speaker task in the clear
613 condition had a small effect size (g* = 0.243 [-0.366, 0.854]; Figure 6F), ranging from a
614 negative medium effect to a positive large effect across participants, and the HPD overlapped
615 0.

616

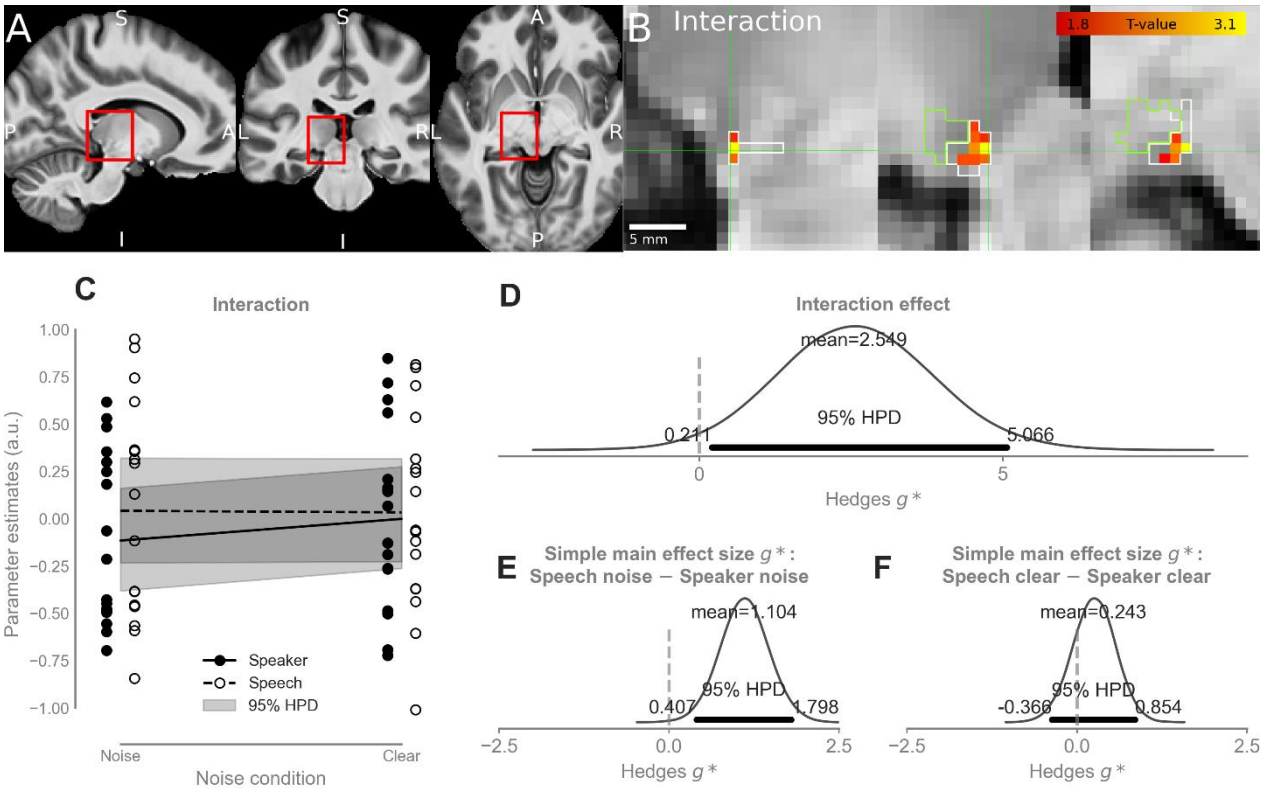

Figure 6. fMRI results. ***A.*** *The mean T1 structural image across participants in MNI space. Red rectangles denote the approximate location of the left MGB and encompass the zoomed-in views in B. Letters indicate anatomical terms of location: A, anterior; P, posterior; S, superior; I, inferior; L, left; R, right. Panels A and B share the same orientation across columns; i.e., from left to right: sagittal, coronal, and axial.* ***B.*** *Statistical parametric map of the interaction (yellow-red colour code): (speech task/noise - speaker task/noise) - (speech task/clear - speaker task/clear) overlaid on the mean structural T1 image. Crosshairs point to MNI coordinate (-11, -28, -6). The white outline shows the boundary of the vMGB mask; the green boundary delineates the non-tonotopic parts of the MGB.* ***C.*** *Parameter estimates (mean-centred) within the vMGB mask. Open circles denote parameter estimates of the speech task condition; filled circles denote parameter estimates of the speaker task condition. Dashed black line: the relationship between noise condition (noise, clear) and parameter estimates in the speech task. Solid black line: the*

relationship between noise condition (noise, clear) and parameter estimates in the speaker task. The shaded grey area shows the 95% HPD. ***D-F*** *Bayesian Analysis of the parameter estimates.* ***D.*** *The effect size of the interaction: the effect size for the interaction effect was very large (2.549 [0.211, 5.066]) and the HPD excluded zero (indicated by the dashed vertical line).* ***E****. Simple main effect: speech task/noise – speaker task/noise. The mean effect size was large (1.104 [0.407, 1.798]). The HPD excluded zero.* ***F****. Simple main effect: speech task/clear – speaker task/clear. The mean effect size was small (0.243 [-0.366, 0.854]). The HPD contained zero.*

The results showed that the task-dependent modulation of the left vMGB for the speech task was increased when participants recognised speech – speaker identity in background noise in contrast to speech – speaker identity without background noise (task × noise interaction). This finding cannot be explained by differences in stimulus input as the same stimulus material was used for the speech and the speaker task. The results are also unlikely due to differences in task difficulty between conditions, as the behavioural results showed no detectable differences in performance for the simple main effects.

We did not have a specific hypothesis on the right vMGB, as there is currently no indication that the task-dependent modulation in this region is behavioural relevant (von Kriegstein et al., 2008; Mihai et al., 2019) or dysfunctional in disorders associated with speech-in-noise processing difficulties (Díaz et al., 2012; Tschentscher et al., 2019). Exploring the interaction in the right vMGB revealed no interaction effect as the HPD strongly overlapped zero (g* = -0.544 [-3.093, 2.459]).

651 ### 3.2.2 Exploratory analyses on the central nucleus of the inferior colliculus (cIC)

652 In exploratory analyses, we investigated the bilateral cIC involvement during speech
653 processing. The reason for these exploratory analyses were studies using auditory brainstem
654 responses (ABR) during passive listening to speech sounds that have shown that the quality
655 of speech sound representation (i.e., as measured by the frequency following response, FFR)
656 explains inter-individual variability in speech-in-noise recognition abilities (Chandrasekaran
657 et al., 2009; Song et al., 2010; Schoof and Rosen, 2016; Selinger et al., 2016). These findings
658 indicated that there might be subcortical nuclei beyond the MGB that are involved in speech-
659 in-noise perception, potentially also sources in the auditory brainstem, particularly the IC
660 (Chandrasekaran and Kraus, 2010b). Four previous fMRI experiments, however, have shown
661 that there is *no* significant task-dependent modulation (i.e., higher BOLD responses for a
662 speech in contrast to a control task on the same stimuli) of the inferior colliculus (von
663 Kriegstein et al., 2008; Díaz et al., 2012; Mihai et al., 2019). Two of them showed a significant
664 positive correlation between the amount of BOLD response difference between a speech and
665 a control task in the left IC and the speech recognition performance across participants (von
666 Kriegstein et al., 2008, experiment 1 and 2), but the others did not. Thus the role of the IC in
667 speech recognition and speech-in-noise recognition is to date unclear. In the present data,
668 there was a small effect of task in the left cIC (speech - speaker, left g*=0.309 [-0.286, 0.902]
669 and right g*= 0.126 [-0.393, 0.646], however, the HPD overlapped zero. The task × noise
670 interaction contained no explanatory power (left: g*=0.049 [-0.103, 0.202], right: g*=-0.010
671 [-0.136, 0.111]) and introduced overfitting. We, therefore, excluded it from the model, and
672 the reported results were computed from the model without an interaction term.

The correlation between the task-dependent modulation (i.e., speech - speaker task contrast) and the speech recognition scores across participants in the left cIC was not significant in the current study (r=0.44, p=0.074, Figure 7).

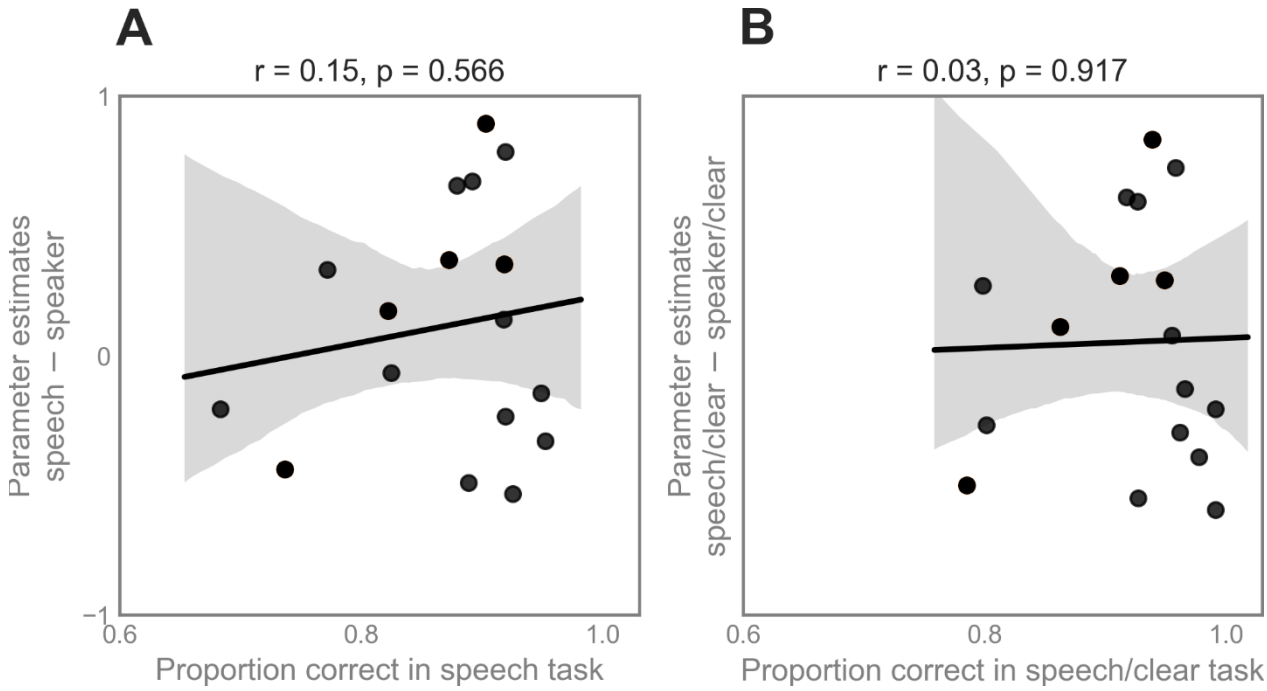

Figure 7. ***A*** *Correlation analysis between the parameter estimates of the contrast Speech – Speaker task in the left cIC and the proportion of hits in the speech task.* ***B*** *Correlation analysis between the parameter estimates of the contrast speech/clear – speaker/clear task in the left cIC and the proportion of hits in the speech/clear task. Most data points are close to the ceiling on the right of the behavioural score. For both correlations, the degrees of freedom were 16.*

684 ## 4. Discussion

685 We showed that the task-dependent modulation for speech of the left hemispheric primary
686 sensory thalamus (vMGB) is particularly strong when recognising speech in noisy listening
687 conditions in contrast to conditions where the speech signal is clear. This finding confirmed
688 our a priori hypothesis which was based on explaining speech-in-noise recognition and
689 sensory thalamus function within a Bayesian brain framework. Exploratory analyses showed
690 that there was no influence of noise on the responses for the contrast between speech and
691 speaker task in the right vMGB, or in the auditory midbrain, i.e., the central nuclei of the
692 inferior colliculi (cIC).

693 Bayesian approaches to brain function propose that the brain uses internal dynamic models
694 to predict the trajectory of the sensory input (Knill and Pouget, 2004; Friston, 2005; Kiebel
695 et al., 2008; Friston and Kiebel, 2009). Thus, slower dynamics of the internal dynamic model
696 (e.g., syllable and word representations) could be encoded by auditory cerebral cortex
697 areas (Giraud et al., 2000; Davis and Johnsrude, 2007; Hickok and Poeppel, 2007; Wang et al.,
698 2008; Mattys et al., 2012; Price, 2012), and provide predictions about the faster dynamics of
699 the input arriving at lower levels of the anatomic hierarchy (Kiebel et al., 2008; von
700 Kriegstein et al., 2008). In this view, dynamic predictions modulate the response properties
701 of the first-order sensory thalamus to optimise the early stages of speech recognition (Mihai
702 et al., 2019). In speech processing, such a mechanism might be especially useful as the signal
703 includes rapid dynamics, that are predictable (e.g., due to co-articulation or learned
704 statistical regularities in words) (Saffran, 2003). In addition, speech often has to be computed
705 online under conditions of (sensory) uncertainty. Uncertainty refers to the limiting reliability

706 of sensory information about the world (Knill and Pouget, 2004). Examples include the
707 density of hair cells in the cochlea that limit frequency resolution, the neural noise-induced
708 at different processing stages, or – as was the case in the current study – background
709 environmental noise that surrounds the stimulus of interest. An internal generative model
710 about the fast sensory dynamics (Knill and Pouget, 2004; Friston, 2005; Kiebel et al., 2008;
711 Friston and Kiebel, 2009) of speech could lead to enhanced stimulus representation in the
712 subcortical sensory pathway and by that provides improved signal quality to the auditory
713 cortex. Such a mechanism would result in more efficient processing when taxing conditions,
714 such as background noise, confront the perceptual system. The interaction between task and
715 noise in the left vMGB is in congruence with such a mechanism. It shows that the task-
716 dependent modulation of the left vMGB is increased in a situation with high sensory
717 uncertainty in contrast to the situation with lower sensory uncertainty. Although the results
718 are in accordance with the Bayesian brain hypothesis, the study was not meant to test
719 directly whether predicticve coding is used in the auditory pathway. To test this it would be
720 necessary to manipulate predictability of the stimuli (Tabas et al., 2020).

721 Both the speech task and the speaker task required attention to the stimuli. Attention can
722 interact to provide a better decoding of the stimuli we choose to attend to (Schröger et al.,
723 2015), and can optimize predictions of incoming signals (Smout et al., 2019) resulting in a
724 top-down and bottom up signal integration (Gordon et al., 2019). Attention can be formulated
725 in a predictive coding account (Ransom et al., 2017), for example, it could result in increased
726 precision on the prediction. It is to date an open question whether the task-dependent
727 modulation observed for speech recognition in the present and previous studies in sensory
728 thalamic nuclei (von Kriegstein et al., 2008; Díaz et al., 2012, 2018; Mihai et al., 2019) operate

729 through the same mechanisms as attentional modulation (O'Connor et al., 2002; Schneider
730 and Kastner, 2009; Schneider, 2011; Ling et al., 2015)

731 Speech-in-noise recognition abilities are thought to rely (i) on additional cognitive resources
732 (reviewed in Peelle, 2018) and (ii) on the fidelity of speech sound representation in
733 brainstem nuclei, as measured by auditory brainstem response recordings (reviewed in
734 Anderson and Kraus, 2010). For example, studies investigating speech-in-noise recognition
735 at the level of the cerebral cortex found networks that include areas pertaining to linguistic,
736 attentional, working memory, and motor planning (Salvi et al., 2002; Scott et al., 2004; Bishop
737 and Miller, 2008; Wong et al., 2008). These results suggested that during speech recognition
738 in challenging listening conditions additional cerebral cortex regions are recruited that likely
739 complement the processing of sound in the core speech network (reviewed in Peelle, 2018).
740 The present study showed that besides the additional cerebral cortex region recruitment, a
741 specific part of the sensory pathway is also modulated during speech-in-noise recognition:
742 the left vMGB.

743 Auditory brainstem response (ABR) recordings during passive listening to speech sounds
744 have shown that the quality of speech sound representation (i.e., as measured by the
745 frequency following response, FFR) explains inter-individual variability in speech-in-noise
746 recognition abilities (Chandrasekaran et al., 2009; Song et al., 2010; Schoof and Rosen, 2016;
747 Selinger et al., 2016) and can be modulated by attention to speech in situations with two
748 competing speech streams (Forte et al., 2017). It is difficult to directly relate the results of
749 these FFR studies on participants with varying speech-in-noise recognition abilities
750 (Chandrasekaran et al., 2009; Song et al., 2010; Schoof and Rosen, 2016; Selinger et al., 2016)
751 to the studies on task-dependent modulation of structures in the subcortical sensory

752 pathway (von Kriegstein et al., 2008; Díaz et al., 2012; Mihai et al., 2019): they involve very
753 different measurement modalities and the FFR studies focus mostly on speech-in-noise
754 perception in passive listening designs. One major candidate for the FFR source is the inferior
755 colliculus. Particularly for speech, the FFR, as recorded by EEG, seems to be dominated by
756 brainstem and auditory nerve sources (reviewed in Chandrasekaran et al., 2014; Bidelman,
757 2018). The results of the present study, however, do not provide evidence for a specific
758 involvement of the inferior colliculus when recognising speech-in-noise. The choice of
759 syllables for the speech task emphasises predictions at the phonetic level. One possibility is
760 that task-dependent modulation of the left MGB in conditions with high sensory uncertainty,
761 might be particularly relevant for such processing at the phonetic level as the MGB might be
762 optimised for this type of fast-varing information (Giraud et al., 2000; von Kriegstein et al.,
763 2008). Whether the inferior colliculus might play a different role in speech-in-noise
764 processing is an open question.

765 We speculate that the task-dependent vMGB modulation might be a result of feedback from
766 cerebral cortex areas. The strength of the feedback could be enhanced when speech has to be
767 recognised in background noise. The task-dependent feedback may emanate directly from
768 primary auditory or association cortices, or indirectly via other structures such as the
769 reticular nucleus with its inhibitory connections to the MGB (Rouiller and de Ribaupierre,
770 1985). Feedback cortico-thalamic projections from layer 6 in A1 to the vMGB, but also from
771 association cortices such as the motion-sensitive planum temporale (Tschentscher et al.,
772 2019), may modulate information ascending through the lemniscal pathway, rather than
773 convey information to the vMGB (Llano and Sherman, 2008; Lee, 2013).

774 Difficulties in understanding speech-in-noise accompany developmental disorders like
775 autism spectrum disorder, developmental dyslexia, and auditory processing
776 disorders (Alcántara et al., 2004; Chandrasekaran et al., 2009; Wong et al., 2009; Ziegler et
777 al., 2009; Bellis and Bellis, 2015; Schoof and Rosen, 2016; Schelinski and Kriegstein, 2019).
778 In the case of developmental dyslexia, previous studies have found that developmental
779 dyslexics do not have the same amount of task-dependent modulation of the left MGB for
780 speech recognition as controls (Díaz et al., 2012) and also do not display the same context-
781 sensitivity of brainstem responses to speech sounds as typical readers (Chandrasekaran et
782 al., 2009). In addition, diffusion-weighted imaging studies have found reduced structural
783 connections between the MGB and cerebral cortex (i.e., the motion-sensitive planum
784 temporale) of the left hemisphere in developmental dyslexics compared to controls (see
785 Müller-Axt et al., 2017 for similar findings in the visual modality; Tschentscher et al., 2019).
786 These altered structures might account for the difficulties in understanding speech-in-noise
787 in developmental dyslexia. Consider distinguishing speech sounds like "dad" and "had" in a
788 busy marketplace. For typically developed individuals, vMGB responses might be modulated
789 to optimally encode the subtle but predictable spectrotemporal cues that enable the explicit
790 recognition of speech sounds. This modulation would enhance speech recognition. For
791 developmental dyslexics, however, this vMGB modulation may be impaired and may explain
792 their difficulty with speech perception in noise (Boets et al., 2007; Ziegler et al., 2009; Díaz et
793 al., 2012).

794 In conclusion, the results presented here suggest that the left vMGB is particularly involved
795 in decoding speech as opposed to identifying the speaker if there is background noise. This
796 enhancement may be due to top-down processes that act upon subcortical sensory

structures, such as the primary auditory thalamus, to better predict dynamic incoming signals in conditions with high sensory uncertainty.

References

Anderson, Samira, and Nina Kraus. 2010. "Sensory-Cognitive Interaction in the Neural Encoding of Speech in Noise: A Review". *Journal of the American Academy of Audiology* 21 (9). American Academy of AAdams RA, Shipp S, Friston KJ (2013) Predictions not commands: active inference in the motor system. Brain Struct Funct 218:611–643.

Adank P (2012) The neural bases of difficult speech comprehension and speech production: Two Activation Likelihood Estimation (ALE) meta-analyses. Brain and Language 122:42–54.

Alavash M, Tune S, Obleser J (2019) Modular reconfiguration of an auditory control brain network supports adaptive listening behavior. PNAS 116:660–669.

Alcántara JI, Weisblatt EJL, Moore BCJ, Bolton PF (2004) Speech-in-noise perception in high-functioning individuals with autism or Asperger's syndrome. Journal of Child Psychology and Psychiatry 45:1107–1114.

Amrhein V, Greenland S, McShane B (2019) Scientists rise up against statistical significance. Nature 567:305.

Anderson AA (2019) Assessing Statistical Results: Magnitude, Precision, and Model Uncertainty. The American Statistician 73:118–121.

Anderson S, Kraus N (2010) Sensory-Cognitive Interaction in the Neural Encoding of Speech in Noise: A Review. Journal of the American Academy of Audiology 21:575–585.

Andersson JLR, Hutton C, Ashburner J, Turner R, Friston K (2001) Modeling Geometric Deformations in EPI Time Series. NeuroImage 13:903–919.

Avants BB, Epstein CL, Grossman M, Gee JC (2008) Symmetric diffeomorphic image registration with cross-correlation: Evaluating automated labeling of elderly and neurodegenerative brain. Medical Image Analysis 12:26–41.

Banno H, Hata H, Morise M, Takahashi T, Irino T, Kawahara H (2007) Implementation of realtime STRAIGHT speech manipulation system: Report on its first implementation. Acoustical Science and Technology 28:140–146.

Baron-Cohen S, Wheelwright S, Skinner R, Martin J, Clubley E (2001) The Autism-Spectrum Quotient (AQ): Evidence from Asperger Syndrome/High-Functioning Autism, Malesand Females, Scientists and Mathematicians. J Autism Dev Disord 31:5–17.

Bastos AM, Usrey WM, Adams RA, Mangun GR, Fries P, Friston KJ (2012) Canonical Microcircuits for Predictive Coding. Neuron 76:695–711.

Bellis TJ, Bellis JD (2015) Central auditory processing disorders in children and adults. Handb Clin Neurol 129:537–556.

Best V, Gallun FJ, Carlile S, Shinn-Cunningham BG (2007) Binaural interference and auditory grouping. The Journal of the Acoustical Society of America 121:1070–1076.

Bidelman GM (2018) Subcortical sources dominate the neuroelectric auditory frequency-following response to speech. NeuroImage 175:56–69.

Bishop CW, Miller LM (2008) A Multisensory Cortical Network for Understanding Speech in Noise. Journal of Cognitive Neuroscience 21:1790–1804.

Boets B, Wouters J, van Wieringen A, Ghesquière P (2007) Auditory processing, speech perception and phonological ability in pre-school children at high-risk for dyslexia: A longitudinal study of the auditory temporal processing theory. Neuropsychologia 45:1608–1620.

Brainard DH (1997) The Psychophysics Toolbox. Spatial Vision 10:433–436.

Bregman AS (1994) Auditory scene analysis: The perceptual organization of sound. MIT press.

Bronkhorst AW (2015) The cocktail-party problem revisited: early processing and selection of multi-talker speech. Atten Percept Psychophys 77:1465–1487.

Bunce JA, McElreath R (2017) Interethnic Interaction, Strategic Bargaining Power, and the Dynamics of Cultural Norms. Hum Nat 28:434–456.

Carhart R, Johnson C, Goodman J (1975) Perceptual masking of spondees by combinations of talkers. The Journal of the Acoustical Society of America 58:S35–S35.

Chandrasekaran B, Hornickel J, Skoe E, Nicol T, Kraus N (2009) Context-dependent encoding in the human auditory brainstem relates to hearing speech in noise: Implications for developmental dyslexia. Neuron 64:311–319.

Chandrasekaran B, Kraus N (2010a) Music, Noise-Exclusion, and Learning. MUSIC PERCEPT 27:297–306.

Chandrasekaran B, Kraus N (2010b) The scalp-recorded brainstem response to speech: Neural origins and plasticity. Psychophysiology 47:236–246.

Chandrasekaran B, Skoe E, Kraus N (2014) An Integrative Model of Subcortical Auditory Plasticity. Brain Topogr 27:539–552.

Chen JJ (2003) COMMUNICATING COMPLEX INFORMATION: THE INTERPRETATION OF STATISTICAL INTERACTION IN MULTIPLE LOGISTIC REGRESSION ANALYSIS. Am J Public Health 93:1376–1377.

Cherry EC (1953) Some Experiments on the Recognition of Speech, with One and with Two Ears. The Journal of the Acoustical Society of America 25:975–979.

Cohen J (1988) Statistical Power Analysis for the Behavioral Sciences, 2nd ed. Lawrence Erlbaum Associates.

Davis KA (2005) Spectral Processing in the Inferior Colliculus. In: International Review of Neurobiology, pp 169–205. Elsevier. Available at: https://linkinghub.elsevier.com/retrieve/pii/S0074774205700064 [Accessed April 3, 2020].

Davis MH, Johnsrude IS (2007) Hearing speech sounds: Top-down influences on the interface between audition and speech perception. Hearing Research 229:132–147.

Denckla MB, Rudel RG (1976) Rapid ‘automatized’ naming (R.A.N.): Dyslexia differentiated from other learning disabilities. Neuropsychologia 14:471–479.

Díaz B, Blank H, von Kriegstein K (2018) Task-dependent modulation of the visual sensory thalamus assists visual-speech recognition. NeuroImage 178:721–734.

Díaz B, Hintz F, Kiebel SJ, Kriegstein K von (2012) Dysfunction of the auditory thalamus in developmental dyslexia. PNAS 109:13841–13846.

Feldman H, Friston K (2010) Attention, Uncertainty, and Free-Energy. Front Hum Neurosci 4 Available at: https://www.frontiersin.org/articles/10.3389/fnhum.2010.00215/full [Accessed March 22, 2019].

Fischl B, Salat DH, van der Kouwe AJW, Makris N, Ségonne F, Quinn BT, Dale AM (2004) Sequence-independent segmentation of magnetic resonance images. NeuroImage 23:S69–S84.

Forte AE, Etard O, Reichenbach T (2017) The human auditory brainstem response to running speech reveals a subcortical mechanism for selective attention Shinn-Cunningham BG, ed. eLife 6:e27203.

Friston K (2005) A theory of cortical responses. Philosophical Transactions of the Royal Society of London B: Biological Sciences 360:815–836.

Friston K, Kiebel S (2009) Predictive coding under the free-energy principle. Philosophical Transactions of the Royal Society of London B: Biological Sciences 364:1211–1221.

Gaudrain E, Li S, Ban VS, Patterson RD (2009a) The Role of Glottal Pulse Rate and Vocal Tract Length in the Perception of Speaker Identity. Interspeech-2009:148–151.

Gaudrain E, Li S, Ban VS, Patterson RD (2009b) The Role of Glottal Pulse Rate and Vocal Tract Length in the Perception of Speaker Identity. In, pp 148–151. Brighton, UK.

Gelman A, Carlin JB, Stern HS, Dunson DB, Vehtari A, Rubin DB, Carlin JB, Stern HS, Dunson DB, Vehtari A, Rubin DB (2013) Bayesian Data Analysis. Chapman and Hall/CRC.

Available at: https://www.taylorfrancis.com/books/9781439898208 [Accessed April 1, 2019].

Gelman A, Hill J (2006) Data analysis using regression and multilevel/hierarchical models. Cambridge university press.

Giraud A-L, Lorenzi C, Ashburner J, Wable J, Johnsrude I, Frackowiak R, Kleinschmidt A (2000) Representation of the Temporal Envelope of Sounds in the Human Brain. Journal of Neurophysiology 84:1588–1598.

Gordon N, Koenig-Robert R, Tsuchiya N, van Boxtel JJ, Hohwy J (2017) Neural markers of predictive coding under perceptual uncertainty revealed with Hierarchical Frequency Tagging. eLife 6 Available at: https://elifesciences.org/articles/22749 [Accessed March 22, 2019].

Gordon N, Tsuchiya N, Koenig-Robert R, Hohwy J (2019) Expectation and attention increase the integration of top-down and bottom-up signals in perception through different pathways. PLOS Biology 17:1–28.

Gorgolewski K, Burns CD, Madison C, Clark D, Halchenko YO, Waskom ML, Ghosh SS (2011) Nipype: A Flexible, Lightweight and Extensible Neuroimaging Data Processing Framework in Python. Front Neuroinform 5 Available at: https://www.frontiersin.org/articles/10.3389/fninf.2011.00013/full [Accessed April 2, 2019].

Griswold MA, Jakob PM, Heidemann RM, Nittka M, Jellus V, Wang J, Kiefer B, Haase A (2002) Generalized autocalibrating partially parallel acquisitions (GRAPPA). Magnetic Resonance in Medicine 47:1202–1210.

Groen WB, van Orsouw L, Huurne N ter, Swinkels S, van der Gaag R-J, Buitelaar JK, Zwiers MP (2009) Intact Spectral but Abnormal Temporal Processing of Auditory Stimuli in Autism. J Autism Dev Disord 39:742–750.

Gupta S, Bhurchandi KM, Keskar AG (2016) An efficient noise-robust automatic speech recognition system using artificial neural networks. In: 2016 International Conference on Communication and Signal Processing (ICCSP), pp 1873–1877.

Han X, Fischl B (2007) Atlas Renormalization for Improved Brain MR Image Segmentation Across Scanner Platforms. IEEE Transactions on Medical Imaging 26:479–486.

Hedges LV, Olkin I (1985) Statistical Methods for Meta-Analysis. Elsevier Science. Available at: https://books.google.de/books?id=brNpAAAAMAAJ.

Hesselmann G, Sadaghiani S, Friston KJ, Kleinschmidt A (2010) Predictive Coding or Evidence Accumulation? False Inference and Neuronal Fluctuations. PLOS ONE 5:e9926.

Hickok G, Poeppel D (2007) The cortical organization of speech processing. Nature Reviews Neuroscience 8:393–402.

Hoffman MD, Gelman A (2014) The No-U-Turn sampler: adaptively setting path lengths in Hamiltonian Monte Carlo. Journal of Machine Learning Research 15:1593–1623.

Huang Y, Rao RPN (2011) Predictive coding. WIREs Cogn Sci 2:580–593.

Iliadou V (Vivian) et al. (2017) A European Perspective on Auditory Processing Disorder-Current Knowledge and Future Research Focus. Front Neurol 8 Available at: https://www.frontiersin.org/articles/10.3389/fneur.2017.00622/full [Accessed June 11, 2019].

Jezzard P, Balaban RS (1995) Correction for geometric distortion in echo planar images from B0 field variations. Magnetic Resonance in Medicine 34:65–73.

Jordan MI ed. (1998) Learning in Graphical Models. Springer Netherlands. Available at: https://www.springer.com/gp/book/9780792350170 [Accessed April 2, 2019].

Kasper L, Bollmann S, Diaconescu AO, Hutton C, Heinzle J, Iglesias S, Hauser TU, Sebold M, Manjaly Z-M, Pruessmann KP, Stephan KE (2017) The PhysIO Toolbox for Modeling Physiological Noise in fMRI Data. Journal of Neuroscience Methods 276:56–72.

Kiebel SJ, Daunizeau J, Friston KJ (2008) A Hierarchy of Time-Scales and the Brain. PLOS Computational Biology 4:e1000209.

Knill DC, Pouget A (2004) The Bayesian brain: the role of uncertainty in neural coding and computation. Trends in Neurosciences 27:712–719.

Kreitewolf J, Gaudrain E, von Kriegstein K (2014) A neural mechanism for recognizing speech spoken by different speakers. NeuroImage 91:375–385.

Lauritzen SL, Dawid AP, Larsen BN, Leimer H-G (1990) Independence properties of directed markov fields. Networks 20:491–505.

Lee CC (2013) Thalamic and cortical pathways supporting auditory processing. Brain and Language 126:22–28.

Lewandowski D, Kurowicka D, Joe H (2009) Generating random correlation matrices based on vines and extended onion method. Journal of Multivariate Analysis 100:1989–2001.

Ling S, Pratte MS, Tong F (2015) Attention alters orientation processing in the human lateral geniculate nucleus. Nat Neurosci 18:496–498.

Llano DA, Sherman SM (2008) Evidence for nonreciprocal organization of the mouse auditory thalamocortical-corticothalamic projection systems. Journal of Comparative Neurology 507:1209–1227.

Marques JP, Kober T, Krueger G, van der Zwaag W, Van de Moortele P-F, Gruetter R (2010) MP2RAGE, a self bias-field corrected sequence for improved segmentation and T1-mapping at high field. NeuroImage 49:1271–1281.

Mattys SL, Davis MH, Bradlow AR, Scott SK (2012) Speech recognition in adverse conditions: A review. Language and Cognitive Processes 27:953–978.

McElreath R (2018) Statistical Rethinking : A Bayesian Course with Examples in R and Stan. Chapman and Hall/CRC. Available at: https://www.taylorfrancis.com/books/9781315362618 [Accessed April 1, 2019].

Mihai PG, Moerel M, de Martino F, Trampel R, Kiebel S, von Kriegstein K (2019) Modulation of tonotopic ventral medial geniculate body is behaviorally relevant for speech recognition. eLife 8:e44837.

Moore BCJ, Peters RW, Glasberg BR (1985) Thresholds for the detection of inharmonicity in complex tones. The Journal of the Acoustical Society of America 77:1861–1867.

Müller-Axt C, Anwander A, von Kriegstein K (2017) Altered Structural Connectivity of the Left Visual Thalamus in Developmental Dyslexia. Current Biology 27:3692-3698.e4.

Mumford D (1992) On the computational architecture of the neocortex. Biol Cybern 66:241–251.

O'Connor DH, Fukui MM, Pinsk MA, Kastner S (2002) Attention modulates responses in the human lateral geniculate nucleus. Nature Neuroscience 5:1203–1209.

Peelle JE (2018) Listening Effort: How the Cognitive Consequences of Acoustic Challenge Are Reflected in Brain and Behavior. Ear and Hearing 39:204.

Price CJ (2012) A review and synthesis of the first 20years of PET and fMRI studies of heard speech, spoken language and reading. NeuroImage 62:816–847.

Ransom M, Fazelpour S, Mole C (2017) Attention in the predictive mind. Consciousness and Cognition 47:99–112.

Rouiller EM, de Ribaupierre F (1985) Origin of afferents to physiologically defined regions of the medial geniculate body of the cat: ventral and dorsal divisions. Hearing Research 19:97–114.

Saffran JR (2003) Statistical Language Learning: Mechanisms and Constraints. Curr Dir Psychol Sci 12:110–114.

Salvatier J, Wiecki TV, Fonnesbeck C (2016) Probabilistic programming in Python using PyMC3. PeerJ Comput Sci 2:e55.

Salvi RJ, Lockwood AH, Frisina RD, Coad ML, Wack DS, Frisina DR (2002) PET imaging of the normal human auditory system: responses to speech in quiet and in background noise. Hearing Research 170:96–106.

Sayles M, Winter IM (2008) Ambiguous Pitch and the Temporal Representation of Inharmonic Iterated Rippled Noise in the Ventral Cochlear Nucleus. J Neurosci 28:11925–11938.

Scharenborg O (2007) Reaching over the gap: A review of efforts to link human and automatic speech recognition research. Speech Communication 49:336–347.

Schelinski S, Kriegstein K von (2019) Speech-in-noise recognition and the relation to vocal pitch perception in adults with autism spectrum disorder and typical development. PsyarXiv Available at: https://psyarxiv.com/u84vd/ [Accessed October 3, 2019].

Schneider KA (2011) Subcortical Mechanisms of Feature-Based Attention. Journal of Neuroscience 31:8643–8653.

Schneider KA, Kastner S (2009) Effects of Sustained Spatial Attention in the Human Lateral Geniculate Nucleus and Superior Colliculus. Journal of Neuroscience 29:1784–1795.

Schneider W, Schlagmüller M, Ennemoser M (2007) LGVT 6-12: Lesegeschwindigkeits-und-verständnistest für die Klassen 6-12. Hogrefe Göttingen.

Schoof T, Rosen S (2016) The Role of Age-Related Declines in Subcortical Auditory Processing in Speech Perception in Noise. JARO 17:441–460.

Schröger E, Marzecová A, SanMiguel I (2015) Attention and prediction in human audition: a lesson from cognitive psychophysiology. Eur J Neurosci 41:641–664.

Scott SK, Rosen S, Wickham L, Wise RJS (2004) A positron emission tomography study of the neural basis of informational and energetic masking effects in speech perception. The Journal of the Acoustical Society of America 115:813–821.

Selinger L, Zarnowiec K, Via M, Clemente IC, Escera C (2016) Involvement of the Serotonin Transporter Gene in Accurate Subcortical Speech Encoding. J Neurosci 36:10782–10790.

Semrud-Clikeman M, Guy K, Griffin JD, Hynd GW (2000) Rapid Naming Deficits in Children and Adolescents with Reading Disabilities and Attention Deficit Hyperactivity Disorder. Brain and Language 74:70–83.

Seth A, Friston K (2016) Active interoceptive inference and the emotional brain. Philosophical Transactions of the Royal Society B: Biological Sciences 371:20160007.

Shinn-Cunningham BG, Best V (2008) Selective Attention in Normal and Impaired Hearing. Trends in Amplification 12:283–299.

Shipp S, Adams RA, Friston KJ (2013) Reflections on agranular architecture: predictive coding in the motor cortex. Trends in Neurosciences 36:706–716.

Smith SM, Jenkinson M, Woolrich MW, Beckmann CF, Behrens TEJ, Johansen-Berg H, Bannister PR, De Luca M, Drobnjak I, Flitney DE, Niazy RK, Saunders J, Vickers J, Zhang Y, De Stefano N, Brady JM, Matthews PM (2004) Advances in functional and structural MR image analysis and implementation as FSL. NeuroImage 23:S208–S219.

Smout CA, Tang MF, Garrido MI, Mattingley JB (2019) Attention promotes the neural encoding of prediction errors. PLOS Biology 17:e2006812.

Song JH, Skoe E, Banai K, Kraus N (2010) Perception of Speech in Noise: Neural Correlates. Journal of Cognitive Neuroscience 23:2268–2279.

Srinivasan MV, Laughlin SB, Dubs A (1982) Predictive coding: a fresh view of inhibition in the retina. Proceedings of the Royal Society of London Series B Biological Sciences 216:427–459.

Tabas A, Mihai G, Kiebel S, Trampel R, Kriegstein K von (2020) Predictive coding underlies adaptation in the subcortical sensory pathway. arXiv preprint Available at: https://arxiv.org/abs/2003.11328v1.

Tschentscher N, Ruisinger A, Blank H, Díaz B, Kriegstein K von (2019) Reduced Structural Connectivity Between Left Auditory Thalamus and the Motion-Sensitive Planum Temporale in Developmental Dyslexia. J Neurosci 39:1720–1732.

Uttl B (2005) Measurement of Individual Differences: Lessons From Memory Assessment in Research and Clinical Practice. Psychol Sci 16:460–467.

Van de Cruys S, Evers K, Van der Hallen R, Van Eylen L, Boets B, de-Wit L, Wagemans J (2014) Precise minds in uncertain worlds: Predictive coding in autism. Psychological Review 121:649–675.

von Kriegstein K, Patterson RD, Griffiths TD (2008) Task-Dependent Modulation of Medial Geniculate Body Is Behaviorally Relevant for Speech Recognition. Current Biology 18:1855–1859.

Wang X, Lu T, Bendor D, Bartlett E (2008) Neural coding of temporal information in auditory thalamus and cortex. Neuroscience 154:294–303.

Wong PCM, Jin JX, Gunasekera GM, Abel R, Lee ER, Dhar S (2009) Aging and cortical mechanisms of speech perception in noise. Neuropsychologia 47:693–703.

Wong PCM, Uppunda, Ajith K., Parrish, Todd B., Dhar, Sumitrajit (2008) Cortical Mechanisms of Speech Perception in Noise. Journal of Speech, Language, and Hearing Research 51:1026–1041.

Yu AJ, Dayan P (2005) Uncertainty, Neuromodulation, and Attention. Neuron 46:681–692.

Ziegler JC, Pech-Georgel C, George F, Lorenzi C (2009) Speech-perception-in-noise deficits in dyslexia. Developmental Science 12:732–745.